

Graphene-Multiwall Carbon Nanotube-Gold Nanocluster Composites Modified Electrode for the Simultaneous Determination of Ascorbic Acid, Dopamine, and Uric Acid

Xiaofang Liu · Shaping Wei · Shihong Chen ·
Dehua Yuan · Wen Zhang

Received: 1 November 2013 / Accepted: 13 May 2014 /
Published online: 23 May 2014
© Springer Science+Business Media New York 2014

Abstract In this paper, graphene-multiwall carbon nanotube-gold nanocluster (GP-MWCNT-AuNC) composites were synthesized and used as modifier to fabricate a sensor for simultaneous detection of ascorbic acid (AA), dopamine (DA), and uric acid (UA). The electrochemical behavior of the sensor was investigated by electrochemical impedance spectroscopy (EIS), cyclic voltammetry (CV) and differential pulse voltammetry (DPV) techniques. The combination of GP, MWCNTs, and AuNCs endowed the electrode with a large surface area, good catalytic activity, and high selectivity and sensitivity. The linear response range for simultaneous detection of AA, DA, and UA at the sensor were 120–1,701, 2–213, and 0.7–88.3 μM , correspondingly, and the detection limits were 40, 0.67, and 0.23 μM (S/N=3), respectively. The proposed method offers a promise for simple, rapid, selective, and cost-effective analysis of small biomolecules.

Keywords Graphene · Multiwall carbon nanotubes · Gold nanoclusters · Ascorbic acid · Dopamine · Uric acid

Introduction

Ascorbic acid (AA), dopamine (DA), and uric acid (UA) usually coexist in biological matrixes, and they were considered as crucial small biomolecules for physiological processes in human metabolism. AA is present in both animal and plant kingdoms, and it is a vital vitamin in human diet and very popular for its antioxidant properties. Moreover, it is also used for the prevention and treatment of common cold, mental illness, infertility, cancer, and AIDS [1, 2]. DA is an important neurotransmitter molecule of catecholamine class which is widely distributed in the mammalian central nervous system for message transfer. It plays a very important role in the function of central nervous, hormonal, renal, and cardiovascular systems [3, 4]. Additionally, low levels of DA may lead to neurological disorders such as Parkinsonism

X. Liu · S. Wei (✉) · S. Chen (✉) · D. Yuan · W. Zhang
Key Laboratory of Luminescent and Real-Time Analytical Chemistry, Ministry of Education, College of Chemistry and Chemical Engineering, Southwest University, Chongqing 400715, People's Republic of China
e-mail: shapingw@swu.edu.cn
e-mail: cshong@swu.edu.cn

and schizophrenia [5]. UA is the primary final product of purine metabolism [6], and its abnormal concentration levels are symptoms of several diseases, such as gout, hyperuricemia, and Lesch-Nyhan disease [7]. Therefore, simultaneous detection of AA, DA, and UA is of critical importance not only in the field of biomedical chemistry and neurochemistry but also in diagnostic applications.

In the past few decades, electrochemical techniques have been receiving considerable interest for the detection of small biomolecules owing to their high sensitivity, rapid response, and low expense. However, there is a challenge to simultaneously determine AA, DA, and UA at substrate electrode because the oxidation potentials of these species are too close to be determined separately, resulting in poor selectivity and sensitivity [8]. In order to overcome this problem, various materials have been employed to modify the electrodes, such as nanoparticles [9–11], polymers [12–17], self-assembled monolayers [18, 19], carbon nanotubes [20–24], and organic redox mediators [25, 26].

Noble metal nanoclusters are a class of materials which were considered as intermediates between noble metal atoms and nanoparticles. They usually consist of several to tens of atoms and are <2 nm in size [27]. Among noble metal nanoclusters, the gold nanoclusters (AuNCs) have drawn wide attention owing to their ultrasmall size, biocompatibility, and nontoxicity. The exploration of AuNCs for sensing applications has spread from metal ions, anions, to small biomolecules [28, 29]. Graphene (GP), a flat monolayer of carbon atoms tightly packed into a 2D honeycomb lattice, possesses high surface area, superior conductivity, and broad potential window. But, GP tends to form irreversible agglomerates or even restocks to form graphite, because the π - π interaction between individual GPs, thus severely restricts its application. To overcome these limitations, a new method should be taken by introducing 1D carbon nanotubes to form a 3D nanohybrid to improve the stability of GP and introduce special functionalities [30]. Additionally, emerged as a good support to make the loaded nanoparticles to achieve a uniform distribution, GP offers a new way to develop hybrid materials [31]. The hybridization of GP with functional nanomaterials usually shows synergistic effects in electrocatalytic applications [32, 33]. For example, a glucose biosensor based on TiO₂-GP composite showed a better catalytic response and a wider linear range for the determination of glucose than GP- or TiO₂-based electrocatalyst [34]. An electrochemical DNA sensor based on the nanogold and reduced GP exhibited an excellent selectivity for the detection of *Listeria monocytogenes* [35].

Based on above observation, in this work, a nanohybrid consisting of GP, multiwalled carbon nanotubes (MWCNTs), and AuNCs was synthesized. The combination of GP, MWCNTs, and AuNCs not only reduces the stacking of GP but also creates a 3D, porous, and conductive catalytic matrix, providing a larger electrochemically active surface area for the adsorption of analytes and effectively facilitating the electron transfer between the electrode and detection molecules. The GP-MWCNTs-AuNCs hybrid was employed to modify electrode for the simultaneous detection of AA, DA, and UA. The electrochemical behaviors of the sensor were investigated by electrochemical impedance spectroscopy (EIS), cyclic voltammetric (CV) and differential pulse voltammetry (DPV).

Experimental

Reagents and Chemicals

AA and DA were purchased from Chongqing Chemical Reagent Co. (Chongqing, China). UA and poly(ethyleneimine) (PEI) were purchased from Sigma Chemical Co. (St. Louis, MO,

USA). Gold chloride (HAuCl_4) was obtained from Shanghai Chemical Reagent Co. (Shanghai, China). MWCNTs (>95 % purity, diameter 20–50 nm, length approximately 2 μm) were purchased from Chengdu Organic Chemicals Co., Ltd. of the Chinese Academy. Graphene oxide (GO) was purchased from Nanjing Xian-feng Nanotechnology Co. (Nanjing, China). Phosphate buffer solutions (PBSs) with various pH were prepared using 0.1 M Na_2HPO_4 and 0.1 M KH_2PO_4 . The supporting electrolyte was 0.1 M KCl. Double-distilled water was used throughout the experiments.

Apparatus

DPV, cyclic voltammetry (CV), and electrochemical impedance spectroscopy (EIS) measurements were performed with CHI660D electrochemical work station (Shanghai Chenhua Instrument Co., China). The conventional three-electrode system included a platinum wire auxiliary electrode, a saturated calomel reference electrode (SCE), and the modified electrode as the working electrodes. Transmission electronmicroscopy (TEM) was carried out on a TECNAI 10 (PHILIPS FEI Co., Holland). The pH measurements were made with a pH meter (MP230, Mettler-Toledo, Switzerland) and a digital ion analyzer (Model PHS-3C, Dazhong Instruments, Shanghai, China). All measurements were carried out at room temperature.

Preparation of GP-MWCNTs-AuNCs

GP-MWCNTs-AuNCs were prepared by the following steps. First, 5.0 mg GO and 5.0 mg MWCNTs were dispersed in 10-mL double-distilled water in an ultrasonic bath. Second, PEI (3 %, 0.2 mL) was added into the suspension (pH 1.0) and heated under reflux at 135 °C for 3 h to obtain the GP-MWCNT composite. Subsequently, 2-mL 1.0 wt% HAuCl_4 was added into 20 mL of 0.2 mg mL^{-1} GP-MWCNTs dispersion. The obtained solution was stirred at 60 °C for 2 h. The resulting product was collected through centrifugation and washed several times using double-distilled water.

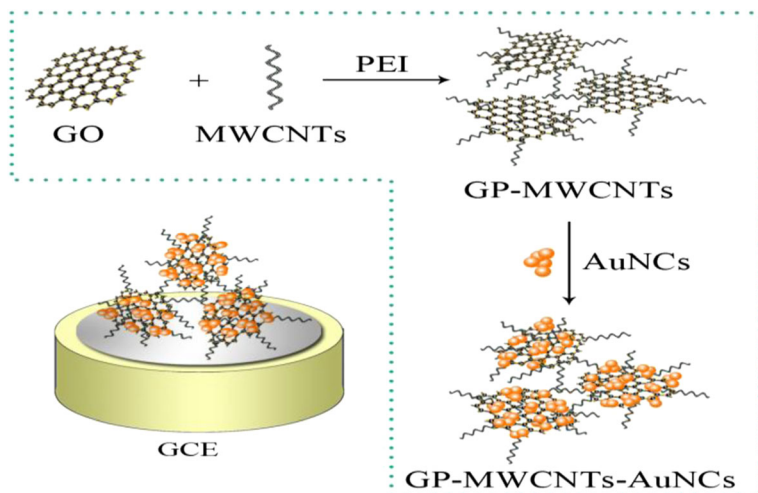
Fabrication of the Sensor

Glassy carbon electrode (GCE, diameter 4.0 mm) was carefully polished with 0.3 and 0.05 μm alumina slurry, respectively, followed by successive ultrasonic with double-distilled water and ethanol until a mirror-like surface was obtained. Then, 10- μL GP-MWCNT-AuNC black suspension (1.0 mg mL^{-1}) prepared by dispersing GP-MWCNTs-AuNCs in double-distilled water with the aid of ultrasonic was dropped on the clean GCE surface and dried in air to obtain the GP-MWCNTs-AuNCs/GCE. Scheme 1 showed the schematic representation of the preparation of GP-MWCNT-AuNC modified electrode. Moreover, for comparison, GP/GCE, MWCNTs/GCE, and GP-MWCNTs/GCE were prepared using the similar procedure for the preparation of GP-MWCNTs-AuNCs/GCE by replacing GP-MWCNTs-AuNCs with GP, MWCNTs, or GP-MWCNTs, respectively.

Results and Discussion

TEM Characterization of GP-MWCNTs-AuNCs

The morphologies and microstructures of GP-MWCNTs and GP-MWCNTs-AuNCs were observed by TEM. As presented in Fig. 1a, sheet structure belonging to the GP was covered



Scheme 1 The schematic representation of the GP-MWCNTs-AuNCs modified electrode

by intertwined MWCNTs, resulting in the formation of the percolating network. As seen from Fig. 1b, the AuNCs with the diameter of 1–3 nm were equably attached to GP-MWCNTs complex. The results indicated that the GP-MWCNT-AuNC nanocomposites were successfully synthesized.

EIS Characterization of the Sensor

EIS can offer useful information on the impedance changes of the electrode surface during the modification process. The typical impedance spectrum (presented in the form of the Nyquist plot) includes a semicircle portion at higher frequencies and a linear part at lower frequency range. The semicircle diameter in the impedance spectrum equals to the electron transfer resistance (R_{ct}). The fabricated process of the modified electrode was monitored by EIS, and the results are presented in Fig. 2. For giving more detailed information about the impedance of the modified electrode, the equivalent circuit model was used to analyze impedance characteristics (insert of Fig. 2). In EIS, the total impedance was determined by several parameters: (1) electrolyte resistance (R_s), (2) Warburg element (Z_w), (3) charge transfer

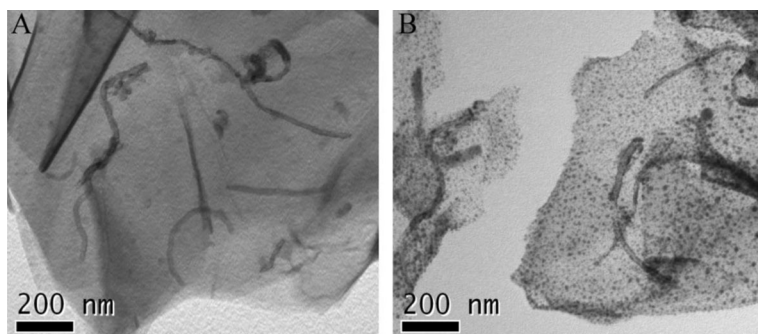


Fig. 1 TEM images of **a** GP-MWCNTs and **b** GP-MWCNTs-AuNCs

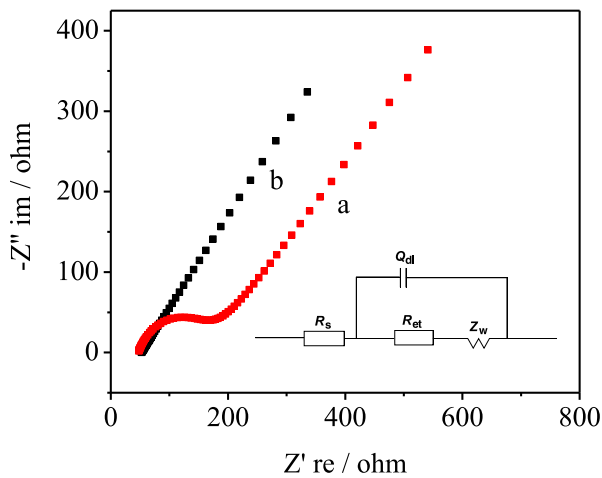


Fig. 2 EIS of **a** bare GCE and **b** GP-MWCNTs-AuNCs/GCE in 5.0 mM $K_3[Fe(CN)_6]/K_4[Fe(CN)_6]$ (1:1) solution

resistance (R_{et}), (4) and the double-layer capacitance (Q_{dl}). The parameters obtained by fitting the equivalent circuit are tabulated in Table 1. The R_s and Z_w represent bulk properties of the electrolyte solution and the diffusion of redox probe, respectively, thus, are not affected by chemical transformations occurring at the electrode surface. Q_{dl} value is related to the roughness of the electrode surface. As seen from Table 1, compared to the bare GCE, the GP-MWCNTs-AuNCs/GCE presented a lower value of n (dispersion coefficient) and a higher value of Q_{dl} , indicating a rougher electrode surface. The value of R_{et} depends on the dielectric and insulating features at the electrode/electrolyte interface. As shown in Fig. 2, when GP-MWCNTs-AuNCs was modified on the GCE (curve b), the semicircle decreased obviously compared to the bare GCE (curve a), and the R_{et} decreased from 126.1 to 6.278 Ω , implying that GP-MWCNTs-AuNCs could accelerate the electron transfer between the electrochemical probe $[Fe(CN)_6]^{4-/3-}$, and the GCE, which is consistent with the fact that GP-MWCNTs-AuNCs is beneficial to the electrons transfer.

Optimization of Detection Conditions

The effect of pH value on the simultaneous determination of AA, DA, and UA at GP-MWCNTs-AuNCs/GCE was investigated by DPV, and the results were shown in Fig. 3a. As seen from Fig. 3a, a maximum peak current of UA was observed at pH 4.0. AA and DA also gave the highest response at pH 4.0. Figure 3b showed the effect of pH on the separation of peak potentials. All the anodic peak potentials for the oxidation of DA, UA, and AA shifted negatively with the increase in the pH, indicating that protons take part in the electrode

Table 1 Values of the equivalent circuit elements from fitted impedance results for bare GCE and GP-MWCNTs-AuNCs/GCE

Electrode	R_s (Ω cm ²)	Z_w (Ω^{-1} cm ⁻² s ^{0.5})	Value of n	R_{et} (Ω cm ²)	Q_{dl} (Ω^{-1} cm ⁻² s ⁿ)
Bare GCE	47.08	2.36×10^{-3}	0.7165	126.1	3.55×10^{-5}
GP-MWCNTs-AuNCs/GCE	52.39	1.86×10^{-3}	0.6214	6.278	1.16×10^{-3}

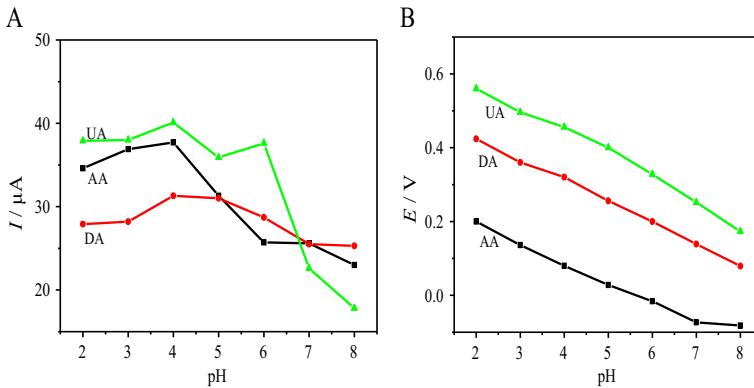


Fig. 3 Effect of pH on **a** the DPV peak currents and **b** the peak potentials for the oxidation of 392 μM AA, 83 μM DA, and 42 μM UA in 0.1 M PBS

reaction processes. The maximum separation of peak potentials for AA–DA and UA–DA is observed at pH 4.0 and 5.0, respectively. In order to obtain a high sensitivity and a good selectivity, pH 4.0 PBS was selected for further experiments.

Electrochemical Behaviors of the Modified Electrodes

The electrochemical behaviors of the different modified electrodes were investigated in 0.1 M PBS (pH 4.0) containing the mixture of 620 μM AA, 52 μM DA, and 64 μM UA and the cyclic voltammograms (CVs) were shown in Fig. 4. As observed, the oxidation peaks of AA, DA, and UA completely overlap, and a broad oxidation peak were observed at 0.5 V at the bare GCE (Fig. 4, curve a), which revealed that it is impossible to simultaneously detect these compounds on bare GCE. Also, these analytes cannot be resolved into individual compound on GP/GCE (Fig. 4, curve b). At the MWCNTs/GCE (Fig. 4, curve c) and GP-MWCNTs/GCE (Fig. 4, curve d), the oxidation peak of DA and UA were observed, and corresponding peak currents were notably improved, indicating a better selectivity than bare GCE. However, the sensitivity is low, and simultaneous determination of AA, DA, and UA could not be obtained

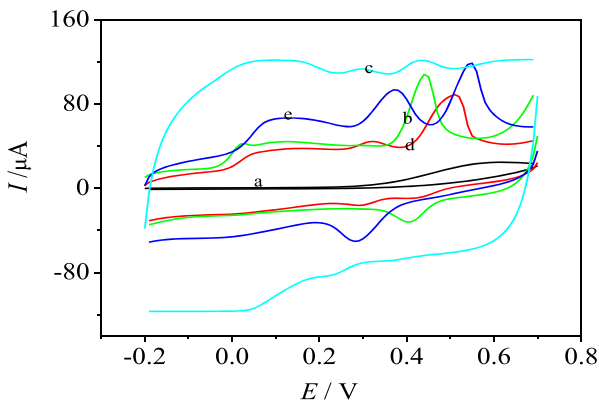


Fig. 4 CVs of **a** bare GCE, **b** GP/GCE, **c** MWCNTs/GCE, **d** GP-MWCNTs/GCE, and **e** GP-MWCNTs-AuNCs/GCE in 0.1 M pH 4.0 PBS containing 620 μM AA, 52 μM DA, and 64 μM UA, respectively

due to the indistinguishable and small response to AA. In contrast, three well-defined voltammetric peaks with a remarkable increase in peak currents were observed at GP-MWCNTs-AuNCs/GCE (Fig. 4, curve e), implying that the discrimination of three species is feasible. The reasons may be as follows: First, MWCNTs not only can accelerate the oxidation of AA, DA, and UA because of the edge of plane graphite and/or defects [36] but also can effectively inhibit the stacking of individual GP and enhance the utilization of GP-based composites. Second, the MWCNTs-GP can increase the effective surface area of modified GCE. Third, AuNCs with excellent electronic conductivity can increase the effective surface area of the modified electrode, thus, enhancing the catalytic activity of MWCNTs-GP/GCE. Based on the synergic effect of MWCNTs, GP and AuNCs facilitating the discrimination of AA, DA, and UA, the modified electrode displayed excellent catalytic activity and selectivity toward the oxidation of AA, DA, and UA.

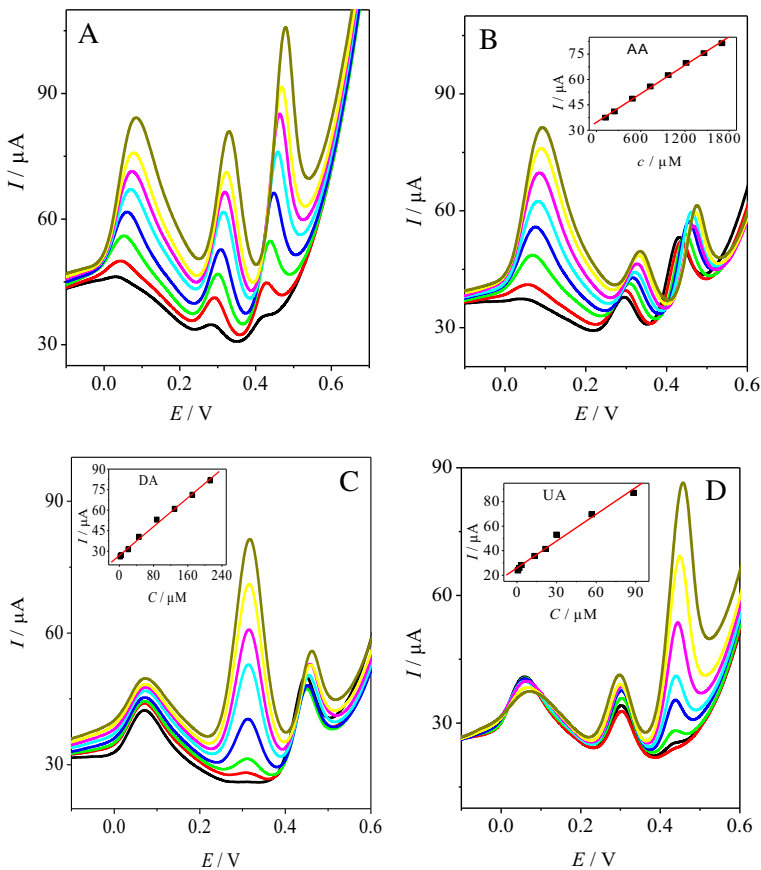


Fig. 5 DPV curves at the GP-MWCNTs-AuNCs/GCE in 0.1 M PBS (pH 4.0) for **a** simultaneous response to AA (125, 250, 450, 650, 850, 1,050, 1,250, and 1,650 μM), DA (8.8, 17.6, 32.4, 47.2, 61.9, 76.6, 91.4, and 120.8 μM), and UA (6.7, 13.3, 20.0, 26.7, 33.3, 40.0, 46.7, and 60.0 μM). **b** containing 50 μM DA, 24 μM UA, and different concentrations of AA (from inner to outer): 120, 243, 486, 729, 972, 1,215, 1,458, 1,701 μM . **c** containing 600 μM AA, 24 μM UA, and different concentrations of DA (from inner to outer): 2, 4, 20, 45, 87, 129, 171, 213 μM . **d** containing 600 μM AA, 62 μM DA, and different concentrations of UA (from inner to outer): 0.7, 1.7, 3.3, 13.3, 21.7, 30, 56.7, and 88.3 μM

Simultaneous Detection of AA, DA, and UA

The primary intention of the present investigation is to simultaneously detect AA, DA, and UA. Figure 5a displayed the DPV curves of different concentration of AA, DA, and UA in the mixture at GP-MWCNTs-AuNCs/GCE. Under optimized conditions, three well-separated and clear peaks were observed. The peak currents for AA, DA, and UA increased linearly with an increase in their respective concentration. This experiment result indicated that the simultaneous discrimination of the three species was feasible. In threefold mixture, the electro-oxidation processes of AA, DA, and UA in the mixture were investigated when the concentration of one species changed, whereas other two species remained constant. Figure 5b showed the DPV curves with varied concentration of AA and constant concentration of DA (50 μM) and UA (24 μM). The linear relationship between the peak current and the concentration of AA was obtained in the concentration range from 120 to 1,701 μM , with the linear function $I_{p,AA} (\mu\text{A})=34.74+0.0281 C_{AA}(\mu\text{M})$ ($R=0.9990$), and a detection limit of 40 μM ($S/N=3$). Figure 5c depicted the DPV curves of DA under a constant concentration of AA (600 μM) and UA (24 μM). The peak current of DA increased linearly with an increase in DA concentration from 2 to 213 μM , with the linear regression equation which was $I_{p,DA} (\mu\text{A})=26.92+0.263 C_{DA} (\mu\text{M})$ ($R=0.9972$) and a detection limit of 0.67 μM ($S/N=3$). Figure 5d illustrated the curves of UA under a constant concentration of AA (600 μM) and DA (62 μM). The linear relationship between the peak current and the concentration of UA was obtained in the concentration range from 0.7 to 88.3 μM with the linear function $I_{p,UA} (\mu\text{A})=25.98+0.728 C_{UA} (\mu\text{M})$ ($R=0.9930$) and a detection limit of 0.23 μM ($S/N=3$). Compared with other reported methods, the GP-MWCNTs-AuNCs/GCE showed a low detection limit, wide linear range, and excellent selectivity and sensitivity. The results were shown in Table 2.

Interferences, Stability, and Reproducibility

To investigate the selectivity of the GP-MWCNTs-AuNCs/GCE, several coexisting compounds were selected. It was found that no significant interference for the detection of AA (200 μM), DA (20 μM), and UA (20 μM) was observed from the following compounds: NaCl (5,000 μM), KCl (5,400 μM), KNO_3 (2,400 μM), NaSO_4 (4,000 μM), glucose (2,500 μM),

Table 2 Comparison of the response characteristics of different modified electrodes

Electrode	Method	Linear response range (μM)			Limit of detection (μM)			Reference
		AA	DA	UA	AA	DA	UA	
HNCMS/electrode	DPV	100–1,000	3.0–75	5.0–30	0.91	0.02	0.04	[37]
OMC-Nafion/GCE	DPV	100–1,000	5.0–50	10–80	20	0.5	4	[38]
poly-EBT/GCE	DPV	150–1,000	0.1–200	10–130	–	–	–	[39]
SZP-MB/electrode	DPV	100–1,600	6–100	22–350	8.3	1.7	3.7	[40]
Chitosan-graphene/GCE	DPV	50–1,200	1.0–24	2.0–45	50	1.0	2.0	[41]
GNP-Ch/GCE	DPV	–	0.2–80	1.2–100	–	0.12	0.6	[42]
GP-MWCNTs-AuNCs/GCE	DPV	120–1,701	2–213	0.7–88.3	40	0.77	0.23	This work

AA ascorbic acid, DA dopamine, UA uric acid, GP graphene, MWCNTs multiwalled carbon nanotubes, AuNCs gold nanoclusters, GCE glassy carbon electrode.

folic acid (200 μM), and L-cysteine (200 μM). The stability of the GP-MWCNTs-AuNCs/GCE was also investigated. The modified electrode was stored at 4 °C in a refrigerator when not in use. The response of GP-MWCNTs-AuNCs/GCE to AA, DA, and UA lost 5.4, 6.3, and 4.7 % of its original response after storage for 7 days, respectively. The reproducibility of the proposed sensors was tested using six different electrodes. The relative standard deviation (RSD) for all these species was less than 4.6 %. Thus, the modified electrode showed an acceptable stability, good repeatability, and anti-interference ability.

Conclusions

The simultaneous determination of AA, DA, and UA is achieved at GP-MWCNTs-AuNCs/GCE in this work. It was found that the modified electrode not only exhibited high electrocatalytic activities toward the oxidation of AA, DA, and UA but also resolved their overlapped oxidation peaks and enhanced the peak currents. With excellent selectivity, good sensitivity, high stability, and wide linear range, the proposed method provides a possibility for simultaneous detection of DA, AA, and UA in biological samples.

Acknowledgments This work is supported by National Natural Science Foundation of China (21075100, 21275119), Municipal Key Laboratory on Luminescence and Real-Time Analysis, Southwest University, and the Fundamental Research Funds for the Central Universities (XDJK2012A004).

References

1. Arrigoni, O., & De Tullio, M. C. (2002). *Biochimica et Biophysica Acta*, 1569, 1–9.
2. Atta, N. F., El-Kady, M. F., & Ahmed, G. (2010). *Analytical Biochemistry*, 400, 78–88.
3. Damier, P., Hirsch, E. C., Agid, Y., & Graybiel, A. M. (1999). *Brain*, 122, 1437–1448.
4. Chakraborty, C., Pal, S., Doss, C. G. P., Wen, Z. H., & Lin, C. S. (2012). *Applied Biochemistry and Biotechnology*, 167, 845–860.
5. Wightman, R. M., May, L. J., & Michael, A. C. (1988). *Analytical Chemistry*, 60, 769A–779A.
6. El Bouhouti, H., Naranjo-Rodríguez, I., de Hidalgo-Hidalgo Cisneros, J. L., ElKaoutit, M., Tamsamani, K. R., Bouchta, D., et al. (2009). *Talanta*, 79, 22–26.
7. Kalimuthu, P., & John, S. A. (2009). *Bioelectrochemistry*, 77, 13–18.
8. Liu, Y., Huang, J. S., Hou, H. Q., & You, T. Y. (2008). *Electrochemistry Communications*, 19, 1431–1434.
9. Huang, J., Liu, Y., Hou, H., & You, T. (2008). *Biosensors and Bioelectronics*, 24, 632–637.
10. Thiagarajan, S., & Chen, S. M. (2007). *Talanta*, 74, 212–222.
11. Zhang, L., & Jiang, X. (2005). *Journal of Electroanalytical Chemistry*, 583, 292–299.
12. Zhang, R., Jin, G. D., Chen, D., & Hu, X. Y. (2009). *Sensors and Actuators B*, 138, 174–181.
13. Balamurugan, A., & Chen, S. M. (2007). *Analytica Chimica Acta*, 596, 92–98.
14. Li, Y. X., & Lin, X. Q. (2006). *Sensors and Actuators B*, 115, 134–139.
15. Nien, P. C., Chen, P. Y., & Ho, K. C. (2009). *Sensors and Actuators B*, 40, 58–64.
16. Su, W. Y., & Cheng, S. H. (2008). *Electrochemistry Communications*, 10, 899–902.
17. Liu, X. F., Zhang, L., Wei, S. P., Chen, S. H., & Lu, Q. Y. (2014). *Biosensors and Bioelectronics*, 57, 232–238.
18. Raj, C. R., Tokuda, K., & Ohsaka, T. (2001). *Bioelectrochemistry*, 53, 183–191.
19. Zhang, L., Jai, J. B., Zou, X. Q., & Dong, S. J. (2004). *Electroanalysis*, 16, 1413–1418.
20. Cui, R. J., Wang, X. Y., Zhang, G. H., & Wang, C. (2012). *Sensors and Actuators B*, 161, 1139–1143.
21. Zhu, S. Y., Li, H. J., Niu, W. X., & Xu, G. B. (2009). *Biosensors and Bioelectronics*, 25, 940–943.
22. Abbaspour, A., & Noori, A. (2011). *Biosensors and Bioelectronics*, 26, 4674–4680.
23. Zhao, Y., Gao, Y., Zhan, D., Liu, H., Zhao, Q., Kou, Y., et al. (2005). *Talanta*, 66, 51–57.

24. Shankaran, D. R., Uehara, N., & Kato, T. (2003). *Analytica Chimica Acta*, 478, 321–327.
25. Zare, H. R., Nasirizadeh, N., & Ardakani, M. M. (2005). *Electrochemistry Communications*, 577, 25–33.
26. Kalimuthu, P., & Abraham John, S. (2009). *Biosensors and Bioelectronics*, 24, 3575–3580.
27. Tao, Y., Li, Y. H., Ren, J. S., & Qu, X. G. (2013). *Biosensors and Bioelectronics*, 42, 41–46.
28. Lin, H., Li, L. J., Lei, C. Y., Xu, X. H., Nie, Z., Guo, M. L., et al. (2013). *Biosensors and Bioelectronics*, 41, 256–261.
29. Wang, X. X., Wu, P., Hou, X. D., & Lv, Y. (2013). *Analyst*, 138, 229–233.
30. Zhang, Y., Yuan, R., Chai, Y. Q., Li, W. J., Zhong, X., & Zhong, H. A. (2011). *Biosensors and Bioelectronics*, 26, 3977–3980.
31. Liu, T., Su, H. C., Qu, X. J., Ju, P., Cui, L., & Ai, S. Y. (2011). *Sensors and Actuators B*, 160, 1255–1261.
32. Zhou, L. Y., Jiang, Y. J., Gao, J., Zhao, X. Q., & Ma, L. (2012). *Applied Biochemistry and Biotechnology*, 168, 1635–1642.
33. Sun, A. L., Sheng, Q. L., & Zheng, J. B. (2012). *Applied Biochemistry and Biotechnology*, 166, 764–773.
34. Jang, H. D., Kim, S. K., Chang, H., Roh, K. M., Choi, J. W., & Huang, J. (2012). *Biosensors and Bioelectronics*, 38, 184–188.
35. Sun, W., Qi, X., Zhang, Y., Yang, H., Gao, H., Chen, Y., et al. (2012). *Electrochimica Acta*, 85, 145–151.
36. Wang, C., Yuan, R., Chai, Y. Q., Chen, S. H., Zhang, Y., Hu, F. X., et al. (2012). *Electrochimica Acta*, 62, 109–115.
37. Xiao, C. H., Chu, X. C., Yang, Y., Li, X., Zhang, X. H., & Chen, J. H. (2011). *Biosensors and Bioelectronics*, 26, 2934–2939.
38. Zheng, D., Ye, J. S., Zhou, L., Zhang, Y., & Yu, C. Z. (2009). *Journal of Electroanalytical Chemistry*, 625, 82–87.
39. Yao, H., Sun, Y. Y., Lin, X. H., Tang, Y. H., & Huang, L. Y. (2007). *Electrochimica Acta*, 52, 6165–6171.
40. Argüello, J., Leidens, V. L., Magosso, H. A., Ramos, R. R., & Gushikem, Y. (2008). *Electrochimica Acta*, 54, 560–565.
41. Han, D. X., Han, T. T., Shan, C. S., Ivaska, A., & Niu, L. (2010). *Electroanalysis*, 22, 2001–2008.
42. Wang, P., Li, Y. X., Huang, X., & Wang, L. (2007). *Talanta*, 73, 431–437.